Subcell Operation and Long-Term Stability Analysis of Perovskite-Based Tandem Solar Cells Using a Bichromatic Light Emitting Diode Light Source

Marko Jošt,* Gašper Matič, Eike Köhnen, Bor Li, Boštjan Glažar, Marko Jankovec, Steve Albrecht, and Marko Topič*

In monolithic tandem solar cells, current—voltage (J—V) characteristics of sub-cells provide invaluable information about their quality and tandem operation. However, accessing the subcell J—Vs is challenging and requires sophisticated spectral methods. Herein, a customized, bichromatic light emitting diode setup (BCLED) for in-depth analysis of tandem solar cells, suitable for subcell operation analysis, and long-term stability testing is presented. For this, two spectrally independent LED arrays are used to selectively bias the two subcells. The power of the developed setup is demonstrated by successfully disentangling the tandem J—V curve into subcell J—V curves. The method is based on a one-diode model for each subcell and is validated by electrical simulations. Afterward, it is used on a fabricated 27.6% efficient perovskite/silicon tandem device, resulting in great agreement with the measured J—V curve. Therefore, the BCLED setup is a versatile tool, suitable for subcell characteristics and long-term stability analysis of tandem solar cells.

1. Introduction

In recent years, perovskite (PVK)-based tandem solar cells have achieved a rapid increase in power conversion efficiency (PCE) and are approaching the predicted PCE of over 32%.[1] The record PCE of PVK/silicon tandem devices is >29%,[2,3] whereas PVK/

Dr. M. Jošt, Dr. G. Matič, Dr. B. Glažar, Dr. M. Jankovec, Prof. M. Topič
Faculty of Electrical Engineering
University of Ljubljana
Tržaška 25, Ljubljana 1000, Slovenia
E-mail: marko.jost@fe.uni-lj.si; marko.topic@fe.uni-lj.si

E. Köhnen, B. Li, Prof. S. Albrecht
Young Investigator Group Perovskite Tandem Solar Cells
Helmholtz-Zentrum Berlin
Kekuléstrasse 5, Berlin 12489, Germany

Prof. S. Albrecht
Faculty IV – Electrical Engineering and Computer Science
Technical University Berlin
Marchstraße 23, Berlin 10587, Germany

PVK and PVK/Cu(In,Ga)Se₂ (CIGS) tandems are not far behind at 24.8%[4] and 24.2%,[3] respectively. Consequently, it is likely that the PVK-based tandem devices will soon enter the photovoltaic (PV) market, for which low cost, large-area processing, and stability in the range of 20—30 years will be of paramount importance. Until now, the stability studies of PVK-based tandems have been rarely reported when compared with their PVK single-junction counterparts. The longest maximum power point (MPP) measurements lasted in the range of several hundred hours, e.g., 400 h for PVK/silicon,[5,6] 500 h for PVK/CIGS,[7] and 500 h for PVK/PVK[4,8] tandem solar cells, compared with more than 1000 h for the single-junction devices.[9–15]

One of the reasons for this is that the reliable measurements used in the stability testing of tandem devices under solar simulators are more complex than the equivalent measurement of single-junction devices. This is due to the serial connection of the subcells in monolithic, two-terminal tandem devices and the fact that the solar simulators usually do not have the exact AM1.5G spectrum. Consequently, the correct light-biasing conditions are often not possible with a single xenon lamp. Instead, a dual halogen/xenon light source or even controllable light emitting diode (LED) light sources are used to make measurements more reliable. The correct calibration of the solar simulator is then conducted based on relative external quantum efficiency (EQE) measurements and two spectrally selective reference solar cells, from which a spectral mismatch correction is calculated independently for each subcell. The entire procedure for setting the correct illumination is iterative and often time-consuming. A more detailed description can be found in the study by Jost et al.[1] Incorrect calibration can result in incorrect short-circuit current density (J_{SC}) and, in particular, fill factor (FF), which are partly determined by the current mismatch between the two subcells.[16,17] Overbiasing of a nonlimiting subcell can mask its poorer performance, such as lower shunt resistance, even though the measured J_{SC} of the tandem cell matches with one obtained from the EQE measurement. In addition, spectral changes due to lamp degradation or incorrect initial mismatch setting can also alter the bias conditions in the subcell and significantly change the stability results.

In field operation and performance monitoring, the current mismatch effect has even greater significance due to the constantly changing solar irradiance and spectrum. Depending on the irradiance and even temperature conditions in the daily cycle, the device may exhibit different current mismatches and even switch from top cell to bottom cell limiting operation or vice versa. Increasing FF slightly compensates for the current loss due to the current mismatch, so this may not critically affect the device.[16] However, the mismatch itself could have a long-term effect on stability. Indeed, it has been shown that PVK single-junction devices are much more stable under MPP tracking than when light soaked in open-circuit conditions,[18] where no net current flows and thus charge extraction is hindered. The accumulated electric charges accelerate the degradation, even more under elevated temperatures. If a prolonged current mismatch occurs, where the PVK cell is not the limiting cell and thus the charges in the PVK layer are not all extracted, the long-term stability of the PVK-based tandems could be affected. It is critical that different mismatch conditions (top cell limiting, bottom cell limiting, current matched) are investigated to determine whether pre-existing mismatch needs to be considered in the fabrication of tandem devices for field operation instead of perfect current matching to ensure the least degrading operation. Standard solar simulators are not suitable for such long-term monitoring setups due to poor control of illumination and the durability of the light source over thousands of hours. Instead, a type of solar simulator that offers durability and spectral flexibility should be used.

In this article, we present a bichromatic light emitting diode (BCLED) light source for long-term stability measurements of tandem solar cells, specifically tailored for PVK-based tandem devices. The BCLED setup consists of two spatially interleaved LED arrays for homogeneous illumination with two wavelengths, blue ($\lambda = 470$ nm) for a top cell and infrared (IR, $\lambda = 940$ nm) light for bottom cell. Both subcells are thus excited independently, allowing independent control of the photocurrents in each of the subcells, which facilitates calibration of the illumination intensity and testing of different bias conditions, i.e., top cell limitation or bottom cell limitation on the same device. In addition to stability testing, BCLED can also be used for subcell selective analyses, e.g., EQE and photoluminescence biasing. Significantly, we demonstrate the procedure for extracting individual subcell $J-V$ curves using BCLED. Due to the series connection of the two subcells in the monolithic architecture, this is otherwise only indirectly accessible via complex methods of bias-dependent quantum efficiency,[19] photoluminescence and electroluminescence measurements,[2,20,21] and light-dependency measurements.[22,23] Compared with these works, our approach is simple and fast, does not require spectrally resolving equipment, and can provide information on true subcell $J-V$ curves including serial losses instead of a pseudocurve. Therefore, we use BCLED to obtain the subcell performance parameters, including open-circuit voltage (V_{OC}) and FF. Knowing these parameters and subcell $J–V$ curves is important information when understanding and improving the tandem performance, or evaluating tandem solar cell degradation, as BCLED can also reveal processing damage in case of underperformance. In addition, we show results of long-term stability analysis of a monolithic PVK/silicon tandem solar cell, which shows excellent stability after 1000 h of illumination and

tracking operation in air, even with improvement of PCE. The developed BCLED is therefore a powerful tool to study the stability of the tandem device and the performance of the individual subcells.

2. Results and Discussion

The BCLED setup is specifically designed for long-term measurements of PVK/silicon tandem devices, with the idea of simplifying the calibration of the light source to the tandem solar cells based on their respective EQE. Therefore, two types of spectrally independent LED arrays were chosen to separately illuminate the subcells: blue LED with a peak wavelength of 470 nm to excite the top cell and IR LED with a peak wavelength of 940 nm to excite the bottom silicon cell. This gives control over setting different photocurrent conditions for the tandem cell and eliminates unwanted current mismatch conditions due to incorrect spectral mismatch of the light source. The bichromatic light source is UV free; however, recently, it has been shown that the blue light has a very similar effect.[24,25] Therefore we expect similar processes to occur in the device under AM1.5 and our bichromatic irradiance.

The BCLED is also suitable for the analysis of PVK/CIGS, PVK/PVK tandem solar cells, or any other tandem technology with complementary bandgaps and similar absorption regions. In principle, other multijunction solar cell technologies with more subcells can also be analyzed in this way, if the LED arrays are adopted. The schematic of the BCLED is shown in cross section in **Figure 1**, whereas the photo of the setup is shown in Figure S1, Supporting Information. The spectra of both LEDs are shown in Figure S2, Supporting Information, along with an example of top and bottom EQE response of the PVK/silicon tandem solar cell, showing that there is no overlap between the two types of LEDs and confirming the independent excitation of
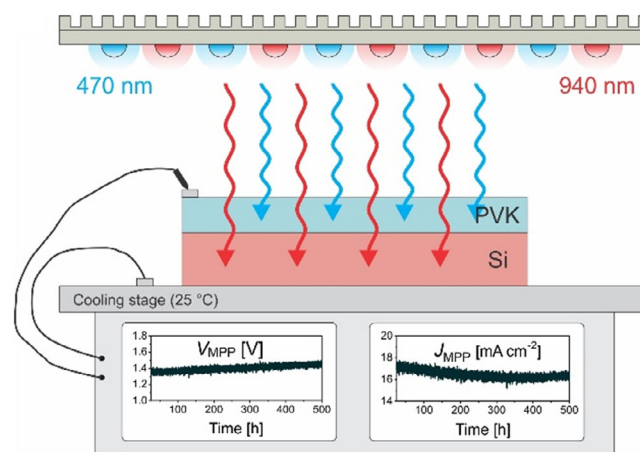

Figure 1. Schematic of the BCLED measurement setup. As the homogeneous illumination source, two sets of LED arrays are used. Blue LEDs with a wavelength of 470 nm (blue) are used to excite the PVK subcell. IR LEDs with a peak wavelength of 940 nm excite the silicon subcell. The sample is placed on a sample holder plate where electrical connections and photodiodes are included for controlling the intensity of the LEDs. In addition, a cooling stage allows to control the cell temperature. For MPP tracking, an in-house developed hardware was used, allowing to track several devices.

each subcell. To ensure uniform illumination over 7.5×7.5 cm^2, a dense LED matrix of 144 blue and 49 IR LEDs was used. The intensity of the LEDs is tracked with spectrally selective photodiodes, separately for blue and IR LEDs. BCLED currently allows simultaneous testing of four thermally connected devices. The system is equipped with a Peltier cooling system for temperature control and an in-house developed μMPP system for MPP tracking of the devices under test.[10,26]

2.1. Subcell Operation Analysis

2.1.1. Performance Parameter Extraction Procedure

One of the main applications with BCLED is the ability to disentangle the $J-V$ curve of the tandem into $J-V$s of subcells and their performance parameters. The parameter extraction procedure is based on a one-diode model for each subcell. For the $J-V$ reconstruction of a single-junction solar cell, the following parameters must first be extracted: series resistance R_S, shunt resistance R_{sh}, saturation current density J_0, and ideality factor n. R_S and R_{sh} can be obtained from a single $J-V$ curve by calculating the slope of the curve at voltages above than open-circuit voltage V_{OC} and at short-circuit conditions, respectively. J_0 and n can be extracted by carrying out a series of $I-V$ measurements at different light intensities and plotting the logarithm of the photocurrent density versus V_{OC} using the following equation, where J_0 and n can be extracted from the line as the intersection with the y-axis and the slope, respectively.

$$\ln(J_L) = \frac{1}{n}\frac{q}{kT}V_{OC} + \ln(J_0) \qquad (1)$$

In a monolithic tandem device parameter, extraction is more challenging because the two subcells are connected in series, which means that we need to extract R_S, R_{sh}, J_0, and n for each subcell, i.e., the top and bottom cell separately. However, these parameters can be reached by biasing each subcell independently with the tunable blue and IR LEDs of the BCLED, which is not possible with conventional solar simulators with one or two lamps. Assuming that one of the devices is strongly biased, we can obtain the necessary parameters of the other, limiting subcell by tuning its light bias in different steps. The changes in performance are then associated with only one subcell, as the other is superimposed as a constant value. Once all parameters are acquired, they can be used in simulations to obtain the $J-V$ curve. The procedure is shown schematically in **Figure 2**. The tandem model schematics, where each subcell is presented with a one-diode model, is shown in **Figure 3**.
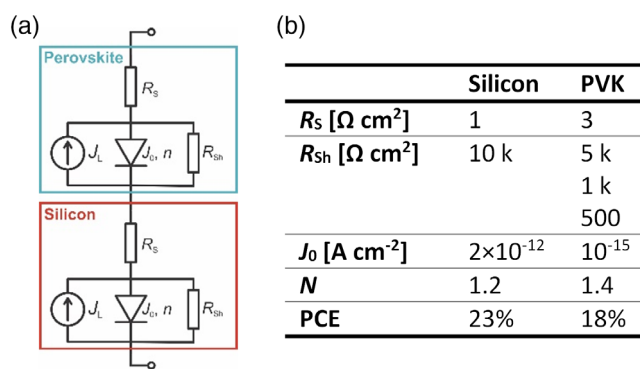

Figure 3. a) Tandem solar cell equivalent circuit model used for simulations, comprising two one-diode models for each subcell. b) Initial input values (series resistance R_S, shunt resistance R_{sh}, ideality factor n, and saturation current density J_0 for electrical simulation parameters for silicon and PVK subcell).

	Silicon	PVK
R_S [Ω cm^2]	1	3
R_{Sh} [Ω cm^2]	10 k	5 k
		1 k
		500
J_0 [A cm^{-2}]	2×10^{-12}	10^{-15}
N	1.2	1.4
PCE	23%	18%

2.1.2. Simulations

The validation of the procedure is first investigated using the simulation software SPICE. The corresponding input parameters for each subcell used for the electrical simulation can be found in Figure 3b, for values of R_S, R_{sh}, J_0, and n. As in typical PVK/silicon tandem solar cells the PVK subcell is more prone to lower (worse) shunt resistance compared with the wafer-based silicon subcell, we chose three different values (500, 1000, and 5000 Ω cm^2) for PVK R_{sh} and conducted the simulations for all three. With the chosen values shown in Figure 3, the silicon single-junction PCE under standard test conditions (STCs) is ≈23% and that of PVK around 19% (for $R_{sh} = 5000$ Ω cm^2), which corresponds to the state-of-the-art PCEs of the tandem subcells. The simulated $J-V$ curves for PVK with $R_{sh} = 1000$ Ω cm^2 are shown in **Figure 4**. In Figure 4a, the PVK subcell is the limiting device and the blue LED intensity (current source J_L) is changed in 4 mA cm^{-2} steps. In Figure 4b, the silicon subcell is the limiting device and therefore the IR LED intensity is changed. In both cases, J_{SC} of the non-limiting subcell is fixed at 25 mA cm^{-2}.

A quick glance at graphs in Figure 4a,b already shows that the lower PVK R_{sh} of the PVK subcell has an impact on the tandem device only in the case where the PVK limits the photocurrent of the tandem device (Figure 4a). Moreover, the tandem R_{sh} is guided by the R_{sh} of the limiting cell, whereas the R_S of the tandem is a sum of the R_{S_pero} and R_{S_Si}. The extracted value of the tandem R_S of 5.5 Ω cm^2 is higher than the value set in the initial parameters (1 Ω cm^2 + 3 Ω cm^2 < 5.5 Ω cm^2), but a more accurate value can be extracted at (much) higher voltages. Nevertheless, the obtained R_S cannot be separated into the individual R_S of the subcells due to

Figure 2. Schematic representation of the procedure to extract parameters and obtain subcell $J-V$ curves of the tandem solar cell.
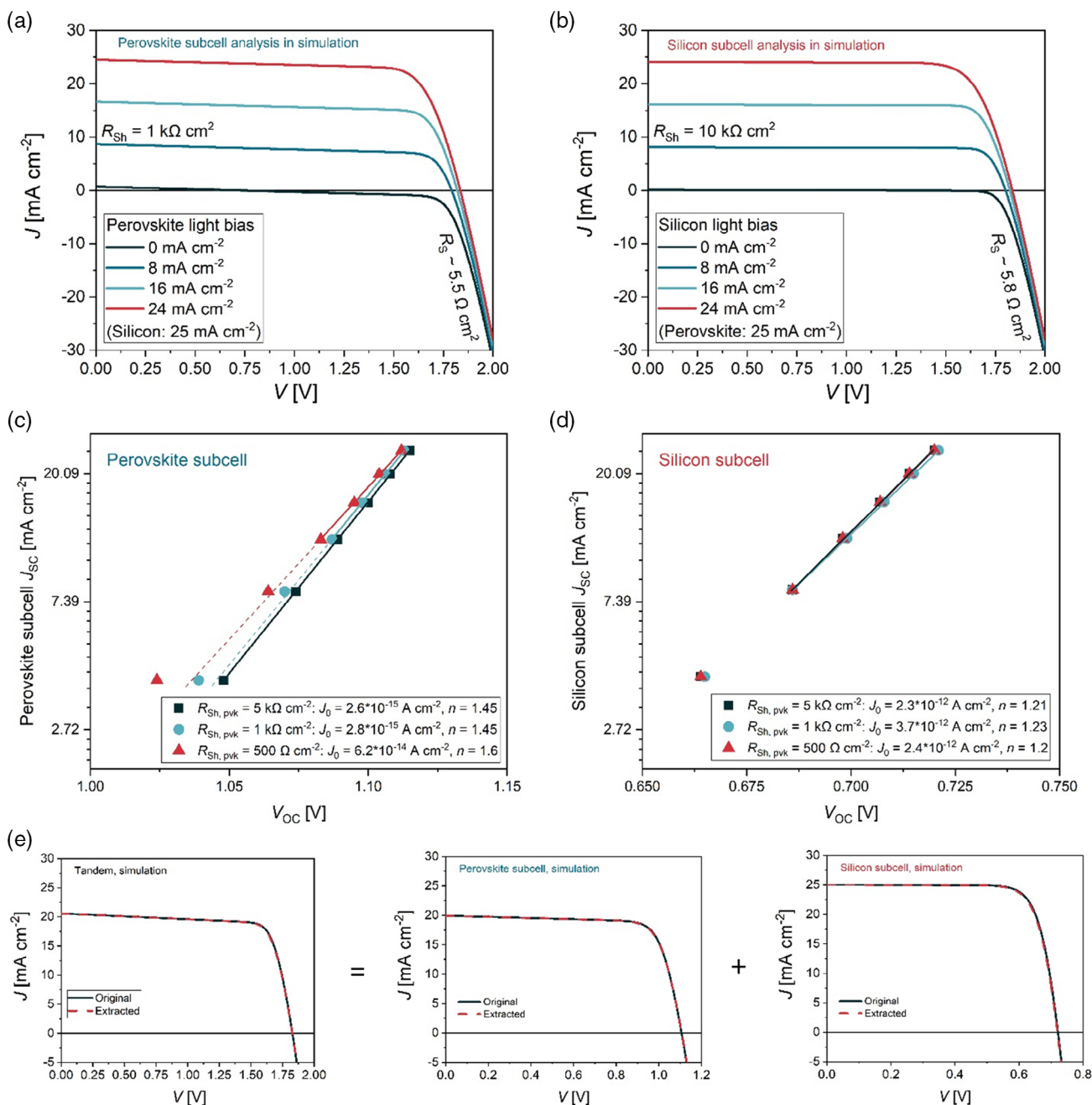
Figure 4. Simulated tandem $J-V$ curves with a) PVK and b) silicon as the photocurrent limiting subcell under different light biases for the limiting cell as indicated by the legend. The nonlimiting cell was biased to 25 mA cm^{-2}. Extracted R_{Sh} and R_S values are also stated. The set values were $R_{Sh} = 1000\ \Omega$ cm^2 and $R_S = 3\ \Omega$ cm^2 for PVK and $R_{Sh} = 10\ k\Omega$ cm^2 and $R_S = 1\ \Omega$ cm^2 for silicon subcell. c,d) I_n (J_{SC}) versus V_{OC} graph from which J_0 and n parameters are extracted from (a) and (b) based on Equation (1) for c) PVK and d) silicon subcell. The x-axis V_{OC} values were obtained by subtracting the V_{OC} of the other subcell (which is the same value for each R_{sh} due to same illumination being applied to the other subcell) from tandem V_{OC}. e) Comparison between simulated tandem (left column), PVK (middle column), and silicon (right column) with initial parameters (black line) and extracted parameters (red line). The initial parameters are stated in Figure 3b. The extracted parameters used to simulate single-junction cells were also extracted from the tandem device and are shown in Figure 4. PVK shunt resistance $R_{sh,top} = 1000\ \Omega$ cm^2.

their series connection. Thus, from the $J-V$s we can easily obtain the R_{sh} of the subcells, whereas for the R_S we can assume that the series resistance of silicon is lower than that of PVKs. Now that we have extracted all four parameters for both subcells, we can reconstruct the tandem $J-V$ and also access the $J-V$s of both subcells.

The results are shown in Figure 4e, where we focused on PVK as the limiting subcell due to its lower R_{sh}, which was set to 1000 Ω cm^2. Black lines show simulations of the tandem device (left) and PVK (middle) and silicon (right) single-junction (subcell) devices with the initial parameters from Figure 3. Red lines show

simulations with the extracted parameters, based on the procedure explained earlier and shown in Figure 4. The graphs are arranged so that the tandem $J-V$ curve (first column) is shown as the sum of the PVK (second column) and silicon $J-V$s (third column), as the top and bottom cell are connected in series. We obtain an excellent agreement, validating our procedure. Even for lower PVK R_{sh} (500 Ω cm^2 in Figure S5, Supporting Information), the agreement is very good. However, there is a slight discrepancy around the MPP point, which extends toward V_{OC} and can also be seen in the deviation of the $J-V$s of both subcells. Therefore, the method can be applied with good accuracy even for cells with poor R_{sh} (<1000 Ω cm^2). For higher R_{sh} the procedure gives excellent agreement.

2.1.3. Experimental Section

We tested the subcell parameter extraction procedure in an experiment on a high-efficiency monolithic PVK/silicon tandem solar cell with a device architecture as published recently.[2] In **Figure 5**, the PVK subcell analysis with measured $I–V$s at different blue LED intensities and fixed IR LED intensity is shown. In Figure S6a,

Supporting Information, the case for silicon subcell analysis is shown. The left panel of Figure 5c shows the measured $I–V$ of the fabricated tandem solar cell under equivalent 1 sun irradiance of BCLED, converting 27.6% of the incident light power into electrical power. To exclude any possible degradation, we conducted a downward and upward intensity test for both subcells: starting from 1.4 sun equivalent blue/IR light intensity and reducing the intensity to 0 and then increasing it back to almost 1.4 suns equivalent. The comparison in Figure S7, Supporting Information, shows no degradation during the test.

Interestingly, the R_{sh} of PVK was not constant throughout the test and ranged from 4.3 kΩ cm^2 for lowest intensities to 1000 Ω cm^2 for highest. Nevertheless, all the values were higher than 1000 Ω cm^2, which we previously set as a limit for successful extraction and reconstruction. The tandem cell R_S was only 3.7 Ω cm^2 assuring high-conversion efficiency under STC conditions. The extracted ideality factors were around 1.2 for both of the subcells (Figure 5b). The extracted value for PVK might seem low; however, we recently extracted a similar value for a PVK single-junction device with a very similar architecture.[10] For J_0 determination, we also need V_{OC} values of the subcells.
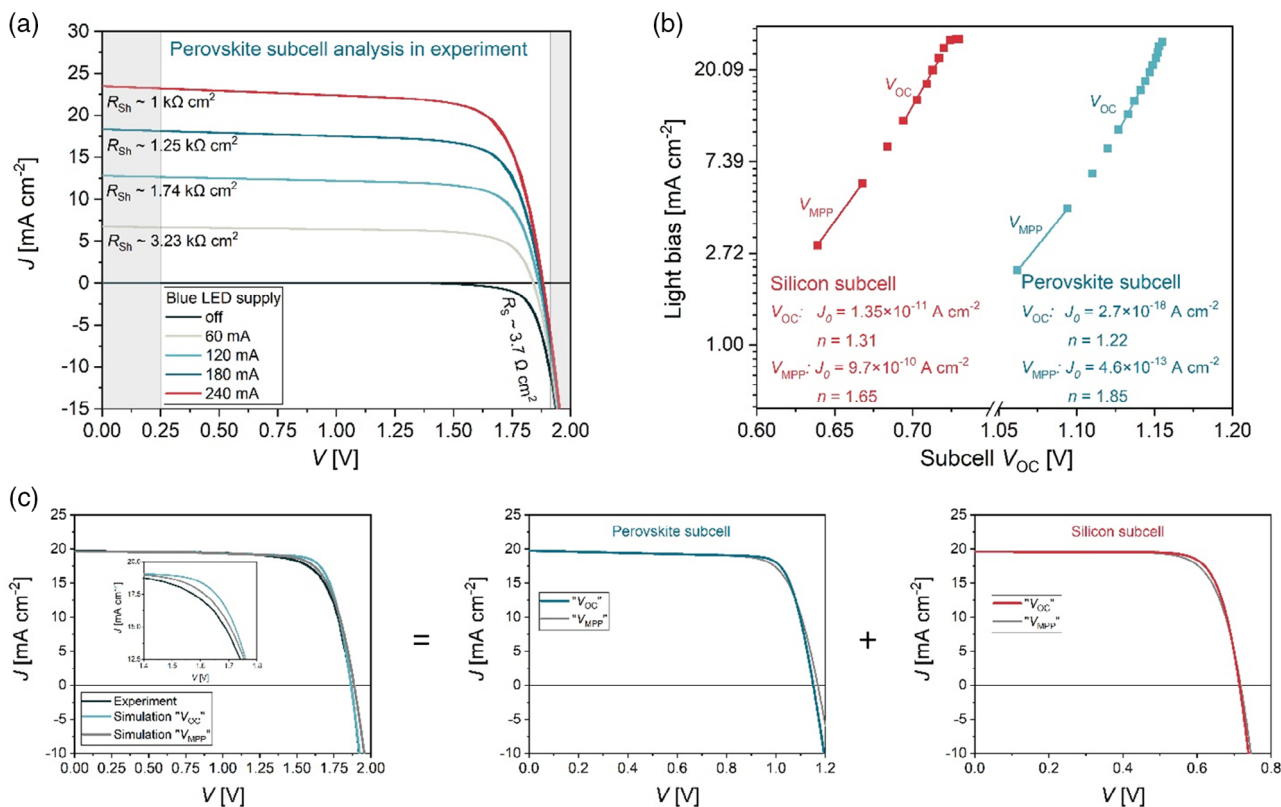

Figure 5. a) BCLED measurement of the fabricated tandem device under constant IR LED intensity and different blue LED intensities. Extracted R_{sh} and R_S are stated with gray areas depicting the range of extraction. b) Light bias versus V_{OC} graph, in which J_0 and n parameters of the fabricated device are extracted. J_0 and n for two cases are stated: "V_{OC}" parameters were extracted from points around the expected V_{OC} of the subcells and "V_{MPP}" at around 90% of the V_{OC} value. The extraction points are labeled with name and line. c) Reconstruction of the single-junction $J–V$s from tandem cell measurement under 1 sun equivalent illumination. Left panel shows comparison between the measurement (black line) and simulation with extracted parameters. Middle and right panel show PVK and silicon single-junction $J–V$ curves that were obtained by simulations with extracted parameters. For all three panels two simulation cases are shown. Colored lines are cases with parameters extracted around V_{OC}, whereas gray lines were obtained with parameters extracted around V_{MPP}. The parameters for the "V_{MPP}" case were also obtained from the measured V_{OC} values, just from a different range (as indicated in the panel b) that is close to V_{MPP} at 1 sun intensity.

V_{OC} of the silicon is easily obtainable, by only turning on the IR LEDs. Interestingly, for PVK, this does not work as by turning only the blue LEDs on, we also see a minor contribution of the silicon subcell, i.e., the measured V_{OC} under such conditions of ≈1.4 V is higher than the expected ≈1.15 V. We postulated that the photoluminescence of PVK gives a small rise to the V_{OC} in silicon, thus influencing our measurement.[27] According to Equation (1), assuming a 0.02% photoluminescence quantum yield of the top cell[2] and half of the emitted light absorbed by the silicon bottom cell, the so-induced V_{OC} in the considered silicon cell would be 450 mV. There is also a possibility that a minor overlap between silicon EQE and the low-energy tail of the blue LED exists, which, however, was not detected by our measurement setups. Nevertheless, this effect is strong only when the bias intensity of the cell in question is very low or zero. For other measurements, this effect plays no role. The PVK subcell V_{OC} can then be obtained by subtracting the silicon subcell V_{OC} from the tandem cell V_{OC}.

With the extracted parameters, the $J{-}V$s shown in Figure 5c were simulated. In the left graph, the comparison between the measurement and simulation with extracted parameters is shown, whereas middle and right graphs show the corresponding PVK and silicon subcell $J{-}V_{s}$. The agreement between the experimental and simulated $J{-}V$ was very good, except around MPP. Such a discrepancy in PVK/silicon tandem devices has been observed before.[16] Here, we attributed it to a nonconstant, voltage-dependent J_0 and n of both subcells in the fabricated device, which can originate i) from the voltage-dependent selectivity at the recombination contact[28] in the fabricated solar cell, as in the simulations, we assumed perfect ohmic connection between the two subcells and/or ii) due to voltage-dependent photocurrent that has also been observed, e.g., in CdTe solar cells.[29] The parameters for the above comparison were extracted around 1 sun V_{OC} voltages for both subcells ("V_{OC}" case), whereas the main discrepancy in the $J{-}V$ curve was around MPP. Therefore, we also extracted J_0 and n parameters from a voltage range that was closer to the MPP value at 1 sun condition, as shown in Figure 5b ("V_{MPP}" case). With these parameters, the matching between experimentally obtained $J{-}V$ and simulated one was much better around MPP but worse around and above V_{OC}. Note that the V_{MPP}s estimated from the "V_{OC}" case were 0.99 and 0.60 V for PVK and silicon subcell, respectively.

By applying our procedure, we could access the $J{-}V$ curves of both subcells. In the middle panel of Figure 5c, the PVK $J{-}V$ is shown, whereas the right one shows $J{-}V$ of the silicon subcell. Both cases are shown, using parameters extracted near V_{OC} (colored lines) and V_{MPP} (gray lines). From the curves, we calculated the subcell performance parameters, which are shown in **Table 1**. The extracted V_{OC}s of the silicon and PVK subcells are 0.715 and 1.151 V, respectively, as obtained from the "V_{OC}" case, matching with the experimentally measured tandem $V_{OC} = 1.866$ V. For FF values, it is more reasonable to consider the "V_{MPP}" extraction case due to a better matching near MPP. Therefore, the FF was 75.8% for both of the subcells and almost the same as measured for the tandem cell (75.3%). Both FF and V_{OC} values were high, proving that both subcells were excellent solar cells, as could have also been deduced from the high PCE of the fabricated tandem device. The earlier results confirm that with our procedure, subcell parameters and their $J{-}V$s are

Table 1. Performance parameters of the measured tandem device and reconstructed PVK and silicon subcells using BCLED extraction procedure. For reconstruction, two sets of parameters were used. First set was obtained around V_{OC} and is labeled as "V_{OC}." Second set was extracted around MPP and is labeled as "V_{MPP}." The expected V_{OC} and FF of the subcell are stated in bold. For V_{OC}, the "V_{OC}" case was considered and for FF, the "V_{MPP}" due to a better fit at the corresponding points in $J{-}V$.

		J_{SC} [mA cm^{-2}]	V_{OC} [V]	FF [%]	PCE [%]
	Tandem (measured)	19.65	1.866	75.3	27.6
"V_{OC}"	PVK	19.75	1.151	79.6	18.1
	Silicon	19.60	**0.715**	78.8	11.0
	V_{OC} sum	–	**1.866**	–	–
"V_{MPP}"	PVK	19.75	1.169	**75.8**	17.5
	Silicon	19.60	0.718	**75.7**	10.7
	V_{OC} sum	–	1.887	–	–

reliably extracted; therefore, the BCLED setup is capable of analyzing instantaneous performance of tandem subcells.

2.2. Stability Measurements

Finally, we used BCLED to test the stability of the fabricated monolithic PVK/silicon tandem solar cell. In this case, a device with a PVK bandgap of 1.62 eV and an initial PCE of 23.1% (as measured under LED class AAA solar simulator) was tested. The stability measurement was carried out in air with an unencapsulated device at 25 °C. The intensities of the blue and IR LEDs were set to reach the equivalent STC photogenerated conditions in both subcells as determined by the EQE measurement (Figure S2, Supporting Information). Results are shown in **Figure 6**, showing a 1000 h MPP track of the monolithic PVK/silicon tandem solar cell, together with V_{MPP} and J_{MPP}. Initial PCE_{MPP} under BCLED was 23.2% and fit well with the
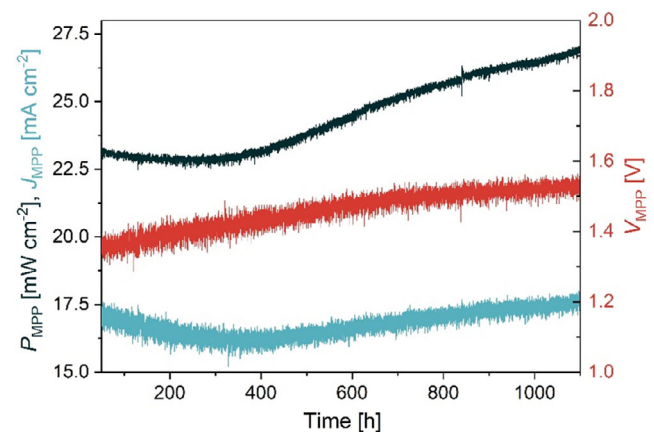

Figure 6. Continuous long-term stability testing using the BCLED setup for more than 1000 h of an unencapsulated monolithic PVK/silicon tandem solar under constant MPP conditions in air. The black curve shows the P_{MPP}, the blue curve shows the J_{MPP} (left y-axis) and the V_{MPP} is shown as red curve (right y-axis).

$PCE_{JV} = 23.1\%$ from $I-V$ measurement under a standard LED sun simulator (see Figure S8, Supporting Information, for $J-V$ curves before and after stability measurement). The PCE_{MPP} remained stable for over 400 h, with only a slight drop in J_{MPP} that was counterbalanced by a V_{MPP} increase. Afterward, surprisingly, the PCE_{MPP} started to increase and reached the PCE of almost 27%. The main reason for this unexpected improvement was the increase in V_{MPP}, which indicated the improvement in V_{OC} and/or FF. This was confirmed by the $I-V$ measurement carried out right after the test. The V_{OC} improved to 1.81 V, whereas the FF increased by 6% absolute to 73.5%. The performance parameters before and after the stability test are compared in Table S2, Supporting Information. As the low FF obtained during the initial measurement is most likely caused by some defects in the PVK top cell, it is possible that longer operation in MPP results in healing those defects as a constant improvement in current, and thus PCE is found after 350 h of constant MPP tracking. Nevertheless, the analysis of origins for the improvement exceeds the scope of this Letter. The PCE measured after the stability test was lower than the PCE from the BCLED. This can indicate that during the short break between the measurements, when the sample had to be transferred from one setup to the other, sample properties changed slightly. Recently, mobile ions have been shown to redistribute within the PVK absorber as a function of applied bias and time, causing changes in performance due to redistribution of the internal field.[30,31] This might have occurred for this sample here as well. Comparing AM1.5G, $I-V$ measurements also reveal that the tandem PCE can be slightly higher in MPP than that extracted from $J-V$ scans, also in the certification laboratory.[2]

3. Conclusion

We have presented a BCLED setup based on two spatially interleaved arrays of blue LEDs with a wavelength of 470 nm and IR LEDs with a wavelength of 940 nm to enable advanced long-term stability testing of tandem solar cells. The independently controlled light intensities make BCLED a powerful tool for a variety of analyses on monolithic tandem solar cells. We have described a procedure to extract the $J-V$ curves of individual subcells in a monolithic tandem device by varying the intensity of the LEDs with a selected wavelength. With this method, the parameters R_{sh}, R_S, J_0, and n of a one-diode model can be extracted for each subcell and used to analyze the tandem device. In this way, invaluable properties about the quality and operation of the subcells are obtained.

The method was validated using simulations for three different shunt resistances of the PVK subcell. Excellent agreement was obtained between the simulations with the initial and extracted parameters for $R_{sh} > 1000\,\Omega\,cm^2$. This procedure was then applied on a high-efficiency fabricated PVK/silicon tandem solar cell. We get a very good agreement between measured and simulated $J-V$ with extracted parameters. The slight discrepancy around the point of maximum power is attributed to the voltage-dependent parameters J_0 and n. With the extracted one-diode parameters, we can also obtain $J-V$ of both subcells and their performance parameters, which provide reliable

in-depth information on the operation of the tandem solar cell and the possible location of damage caused by processing.

In addition, the BCLED setup has been used for long-term stability measurements of tandem devices, as demonstrated by conducting a 1000 h stability test. The longer operating times of the LEDs and the ease of calibration are two of the main advantages of the system. Due to the ease of changing the subcell bias, the setup can be used to test different tandem conditions, such as stability under blue-rich or blue-deficient irradiance. We believe that the presented advantages of the bichromatic light source will promote new interesting results on PVK-based and also other tandem technologies.

Conflict of Interest

The authors declare no conflict of interest.

Data Availability Statement

The data that supports the findings of this study are available in the supplementary material of this article.

[1] M. Jošt, L. Kegelmann, L. Korte, S. Albrecht, *Adv. Energy Mater.* **2020**, *10*, 1904102.

[2] A. Al-Ashouri, E. Köhnen, B. Li, A. Magomedov, H. Hempel, P. Caprioglio, J. A. Márquez, A. B. M. Vilches, E. Kasparavicius, J. A. Smith, N. Phung, D. Menzel, M. Grischek, L. Kegelmann, D. Skroblin, C. Gollwitzer, T. Malinauskas, M. Jošt, G. Matič, B. Rech, R. Schlatmann, M. Topič, L. Korte, A. Abate, B. Stannowski, D. Neher, M. Stolterfoht, T. Unold, V. Getautis, S. Albrecht, *Science* **2020**, *370*, 1300.

[3] Best Research-Cell Efficiency Chart | Photovoltaic Research | NREL, https://www.nrel.gov/pv/cell-efficiency.html (accessed: April 2021).

[4] R. Lin, K. Xiao, Z. Qin, Q. Han, C. Zhang, M. Wei, M. I. Saidaminov, Y. Gao, J. Xu, M. Xiao, A. Li, J. Zhu, E. H. Sargent, H. Tan, *Nat. Energy* **2019**, *4*, 864.

[5] F. Sahli, J. Werner, B. A. Kamino, M. Bräuninger, R. Monnard, B. Paviet-Salomon, L. Barraud, L. Ding, J. J. D. Leon, D. Sacchetto, G. Cattaneo, M. Despeisse, M. Boccard, S. Nicolay, Q. Jeangros, B. Niesen, C. Ballif, *Nat. Mater.* **2018**, *17*, 820.

[6] Y. Hou, E. Aydin, M. D. Bastiani, C. Xiao, F. H. Isikgor, D.-J. Xue, B. Chen, H. Chen, B. Bahrami, A. H. Chowdhury, A. Johnston, S.-W. Baek, Z. Huang, M. Wei, Y. Dong, J. Troughton, R. Jalmood, A. J. Mirabelli, T. G. Allen, E. V. Kerschaver, M. I. Saidaminov, D. Baran, Q. Qiao, K. Zhu, S. D. Wolf, E. H. Sargent, *Science* **2020**, *367*, 1135.

[7] Q. Han, Y.-T. Hsieh, L. Meng, J.-L. Wu, P. Sun, E.-P. Yao, S.-Y. Chang, S.-H. Bae, T. Kato, V. Bermudez, Y. Yang, *Science* **2018**, *361*, 904.

[8] A. F. Palmstrom, G. E. Eperon, T. Leijtens, R. Prasanna, S. N. Habisreutinger, W. Nemeth, E. A. Gaulding, S. P. Dunfield, M. Reese, S. Nanayakkara, T. Moot, J. Werner, J. Liu, B. To, S. T. Christensen, M. D. McGehee, M. F. A. M. van Hest, J. M. Luther, J. J. Berry, D. T. Moore, *Joule* **2019**, *3*, 2193.

[9] J. Xu, C. C. Boyd, Z. J. Yu, A. F. Palmstrom, D. J. Witter, B. W. Larson, R. M. France, J. Werner, S. P. Harvey, E. J. Wolf, W. Weigand, S. Manzoor, M. F. A. M. van Hest, J. J. Berry, J. M. Luther, Z. C. Holman, M. D. McGehee, *Science* **2020**, *367*, 1097.

[10] M. Jošt, B. Lipovšek, B. Glažar, A. Al-Ashouri, K. Brecl, G. Matič, A. Magomedov, V. Getautis, M. Topič, S. Albrecht, *Adv. Energy Mater.* **2020**, *10*, 2000454.

[11] R. Prasanna, T. Leijtens, S. P. Dunfield, J. A. Raiford, E. J. Wolf, S. A. Swifter, J. Werner, G. E. Eperon, C. de Paula, A. F. Palmstrom, C. C. Boyd, M. F. A. M. van Hest, S. F. Bent, G. Teeter, J. J. Berry, M. D. McGehee, *Nat. Energy* **2019**, *4*, 939.

[12] S. Chen, Y. Liu, X. Xiao, Z. Yu, Y. Deng, X. Dai, Z. Ni, J. Huang, *Joule* **2020**, *4*, 2661.

[13] E. H. Jung, N. J. Jeon, E. Y. Park, C. S. Moon, T. J. Shin, T.-Y. Yang, J. H. Noh, J. Seo, *Nature* **2019**, *567*, 511.

[14] S. Yang, S. Chen, E. Mosconi, Y. Fang, X. Xiao, C. Wang, Y. Zhou, Z. Yu, J. Zhao, Y. Gao, F. D. Angelis, J. Huang, *Science* **2019**, *365*, 473.

[15] H. Tsai, R. Asadpour, J.-C. Blancon, C. C. Stoumpos, O. Durand, J. W. Strzalka, B. Chen, R. Verduzco, P. M. Ajayan, S. Tretiak, J. Even, M. A. Alam, M. G. Kanatzidis, W. Nie, A. D. Mohite, *Science* **2018**, *360*, 67.

[16] E. Köhnen, M. Jošt, A. B. Morales-Vilches, P. Tockhorn, A. Al-Ashouri, B. Macco, L. Kegelmann, L. Korte, B. Rech, R. Schlatmann, B. Stannowski, S. Albrecht, *Sustainable Energy Fuels* **2019**, *3*, 1995.

[17] M. Boccard, C. Ballif, *ACS Energy Lett.* **2020**, *5*, 1077.

[18] B. Chen, J. Song, X. Dai, Y. Liu, P. N. Rudd, X. Hong, J. Huang, *Adv. Mater.* **2019**, *31*, 1902413.

[19] J. Gilot, M. M. Wienk, R. A. J. Janssen, *Adv. Funct. Mater.* **2010**, *20*, 3904.

[20] S. Roensch, R. Hoheisel, F. Dimroth, A. W. Bett, *Appl. Phys. Lett.* **2011**, *98*, 251113.

[21] D. Alonso-Álvarez, N. Ekins-Daukes, *IEEE J. Photovoltaics* **2016**, *6*, 1004.

[22] A. R. Jeong, S. B. Choi, W. M. Kim, J.-K. Park, J. Choi, I. Kim, J. Jeong, *Sci. Rep.* **2017**, *7*, 15723.

[23] Y. Tsuno, Y. Hishikawa, K. Kurokawa, in *Conf. Rec. Thirty-First IEEE Photovolt. Spec. Conf. 2005*, **2005**, pp. 1476–1479.

[24] N. H. Nickel, F. Lang, V. V. Brus, O. Shargaieva, J. Rappich, *Adv. Electron. Mater.* **2017**, *3*, 1700158.

[25] A. Farooq, M. R. Khan, T. Abzieher, A. Voigt, D. C. Lupascu, U. Lemmer, B. S. Richards, U. W. Paetzold, *ACS Appl. Energy Mater.* **2021**, *4*, 3083.

[26] LPVO: Cell monitoring, http://lpvo.fe.uni-lj.si/en/services/pv-monitoring/cell-monitoring/ (accessed: April 2021).

[27] A. R. Bowman, F. Lang, Y.-H. Chiang, A. Jiménez-Solano, K. Frohna, G. E. Eperon, E. Ruggeri, M. Abdi-Jalebi, M. Anaya, B. V. Lotsch, S. D. Stranks, *ACS Energy Lett.* **2021**, 612.

[28] M. D. Bastiani, A. S. Subbiah, E. Aydin, F. H. Isikgor, T. G. Allen, S. D. Wolf, *Mater. Horizons* **2020**, *7*, 2791.

[29] S. Hegedus, D. Desai, C. Thompson, *Prog. Photovoltaics Res. Appl.* **2007**, *15*, 587.

[30] K. Domanski, B. Roose, T. Matsui, M. Saliba, S.-H. Turren-Cruz, J.-P. Correa-Baena, C. R. Carmona, G. Richardson, J. M. Foster, F. D. Angelis, J. M. Ball, A. Petrozza, N. Mine, M. K. Nazeeruddin, W. Tress, M. Grätzel, U. Steiner, A. Hagfeldt, A. Abate, *Energy Environ. Sci.* **2017**, *10*, 604.

[31] E. C. Smith, C. L. C. Ellis, H. Javaid, L. A. Renna, Y. Liu, T. P. Russell, M. Bag, D. Venkataraman, *J. Phys. Chem. C* **2018**, *122*, 13986.